Upconverting Nanoparticle to Quantum Dot Förster Resonance Energy Transfer: Increasing the Efficiency through Donor Design

Riccardo Marin[a,b,†], Lucía Labrador-Paéz[c], Artiom Skripka[a], Patricia Haro-González[c], Antonio Benayas[a,d], Patrizia Canton[b], Daniel Jaque*[c,e] and Fiorenzo Vetrone*[a,f]

[a] Institut National de la Recherche Scientifique, Centre Énergie Matériaux Télécommunications (INRS - EMT), Université du Québec, 1650 Boul. Lionel-Boulet, Varennes, Québec, J3X 1S2, Canada

[b] Dipartimento di Scienze Molecolari e Nanosistemi, Università Ca' Foscari, Venezia, Via Torino 155/B - 30172 Venezia-Mestre, Italy

[c] Fluorescence Imaging Group, Departamento de Física de Materiales, and Instituto Nicolás Cabrera, Facultad de Ciencias, Universidad Autónoma de Madrid, 28049 Madrid, Spain

[d] Department of Physics and CICECO – Aveiro Institute of Materials, University of Aveiro, 3810-193, Aveiro, Portugal

[e] Instituto Ramón y Cajal de Investigación Sanitaria, IRYCIS, Ctra. Colmenar km. 9.100, Madrid 28034, Spain

[f] Centre for Self-Assembled Chemical Structures, McGill University, Montréal, Québec, H3A 2K6, Canada

KEYWORDS: FRET, energy transfer, upconversion, quantum dots, nanoparticles, core-shell, copper indium sulfide, $CuInS_2$, $LiYF_4$

ABSTRACT: We propose two effective approaches to enhance the Förster resonance energy transfer (FRET) efficiency from near-infrared (NIR) excited upconverting nanoparticles (UCNPs, namely $LiYF_4$:Yb^{3+},Tm^{3+}) to $CuInS_2$ quantum dots (QDs) upon engineering of the donor's architecture. The study of the particles' interaction highlighted a radiative nature of the energy transfer (ET) among the moieties under investigation when in solution. However, analyses performed on dry powders allowed to observe clear evidence of a FRET mechanism. In particular, photoluminescence lifetime measurements showed that FRET efficiency could be effectively increased by, both, reducing the size of the UCNPs and directly controlling the distribution of the active ions throughout the donor's volume, *i.e.* doping them only in the outer shell of a core/shell system. Both strategies resulted at least in a more than doubled FRET efficiency compared to larger core-only UCNPs. Obtained experimental values were compatible with those predicted from geometrical considerations on the active ions' distribution over the UCNP volume. These results provide a concrete proof of the potential of UCNP-QD FRET pair when the system is properly designed, hence setting a solid base for the development of robust and efficient all-inorganic probes for FRET-based assays.

Introduction

Förster resonance energy transfer (FRET) is a non-radiative energy transfer (ET) process between two optically-active species (donor and acceptor) that is triggered by light [1]: after the radiation is absorbed by the donor, the energy is passed to the acceptor without the involvement of any photon. Overall, this mechanism leads to the donor's emission quenching and possibly to the appearance of the acceptor's luminescent signal. Notably, FRET is a short-range phenomenon whose effects are usually observed in the 0-10 nm donor-acceptor separation range, a fact that directly stems from the dipole-dipole nature of the interaction between the moieties [2]. Therefore, FRET is a powerful tool to probe events occurring at the nanoscale through an easily detectable optical signal, overcoming the theoretical spatial resolution limit achievable with visible electromagnetic radiation.

FRET has been successfully exploited to investigate the short-scale interaction between chemical species [3, 4] and applied in biology for a number of all-optical assays [5-9]. "Classical" FRET techniques take advantage of intermolecular interactions, in particular those occurring among dyes and/or metal complexes [10]. Nonetheless, these techniques suffer from the typical shortcomings that affect organic dye-based methods, *e.g.* photobleaching, short-lived emission (that makes it hard to clearly discern the dye's signal from the autofluorescence of biological components), spectral cross-talk between moieties, poor chemical stability, and often pH dependent optical properties [11, 12]. Neither the later advent of green fluorescent protein (GFP) and its derivatives allowed to overcome the drawbacks of short emission lifetime (LT) and broad absorption/emission bands [13]. Hence, the applicability of FRET-based assays in intracellular milieus, albeit highly attractive and widely spread, remains practically challenging.

More recently, nanoparticles (NPs) have made their appearance in the field as both potential energy donors and acceptors, opening a wide spectrum of new possibilities [14-21]. Among others, upconverting NPs (UCNPs) are alluring energy donors in the frame of FRET [22-25]. Their appeal resides in a long-lived visible emission triggered by near-infrared (NIR) excitation, which allows to overcome the autofluorescence of biological media [26]. Moreover, NIR operational capabilities are of great interest when sub-cutaneous applications are sought, since in this spectral range light scattering and absorption phenomena in biological tissues are minimized [27, 28]. Although UCNPs' low photoluminescence quantum yield (PLQY) has curbed their applicability in FRET-based assays, the exploitation of Gd^{3+}-mediated energy migration throughout the UCNP's volume [25], as well as core/shell engineering [29-31] were recently proven as effective means to control UCNPs' optical properties and circumvent their limitations in the frame of FRET.

Works proposing UCNPs as FRET donors mainly involve the use of acceptors such as organic dyes [32,33], carbon-based systems [34] or gold NPs [35,36]. Despite the considerable literature on the subject, the combination of UCNPs and QDs as a donor-acceptor pair is largely unexplored. This pair has the potential to become a robust all-inorganic FRET system widely applied in optical assays; indeed, the combined advantages of UNCPs' NIR excitation and long-lived emission, along with QDs' broadband absorption are paramount assets. Moreover, these features come bundled with the superior photo and chemical stability granted by both inorganic species.

The study of this type of systems is still in its infancy, leaving plenty of room for investigation both at the level of material optimization and application. Following the path initiated by the first studies on the subject [32, 37, 38], the seminal report on FRET between UCNPs and QDs was published by Bednarkiewicz *et al.* in 2010 [39]. The authors studied the ET from $NaYF_4$:Yb^{3+},Er^{3+} UCNPs to CdSe QDs, reporting a FRET efficiency of approximately 15%. To the best of our knowledge, few papers on similar systems were published since then. These studies confirmed the potential of the UCNP-QD FRET pair applied in *e.g.* biotin [40] and oligonucleotide detection [41], or as an effective NIR detection system [42]. Although these promising observations, there is a lack of careful investigation about the fundamental physical aspects governing FRET among UCNPs and QDs, while a thorough optimization of the architecture/geometry of the pair is currently missing.

Here, we have sought to investigate the effect that the UCNP size, as well as the distribution of the active ions in the UCNP volume, has on the FRET efficiency to QDs. $LiYF_4$:Yb^{3+},Tm^{3+} and $CuInS_2$ (CIS) were the selected materials to prepare UCNPs (donors) and QDs (acceptors), respectively. The rationale underlying the choice of the upconverting material is the strong ultraviolet (UV)-blue upconversion luminescence (UCL) stemming from $LiYF_4$ doped with Yb^{3+} (sensitizer) and Tm^{3+} (activator) ions, that considerably overlaps with ternary CIS QD broadband absorption. Moreover, newly emerging CIS QDs were preferred over "traditional" binary QDs for two reasons: CIS QDs' optical properties can be tuned with ease to ensure NIR operational capabilities and they are free of toxic heavy metal ions (contrary to most high quality binary QDs). Both features are extremely valuable when foreseeing the possibility of using the system in biological environments. Overall, we give a comprehensive insight about the most relevant factors determining FRET from UCNP to QD, in order to provide a solid background for new advancements in the field.

Experimental section

Chemicals

Yttrium oxide (Y_2O_3, 99.99+%), ytterbium oxide (Yb_2O_3, 99.99+%), thulium oxide (Tm_2O_3, 99.99+%), trifluoroacetic acid (TFA, 99%), lithium trifluoroacetate (LiTFA, 97%), indium acetate ($In(OAc)_3$, 99.99%), oleic acid (OA, 90%, Alfa Aesar), 1-octadecene (ODE, 90%), hexane (99%) were purchased from Alfa Aesar. Copper (I) iodide (CuI, 98%), oleylamine (OLAm, 70%), 1-dodecanethiol (DDT, 98+%), toluene (99%) and acetone (99%) were purchased from Aldrich. Ethanol (99%) was obtained from Commercial Alcohols. All chemicals were used as received.

Nanoparticle synthesis

Large $LiYF_4$:Yb^{3+},Tm^{3+} UCNPs (*L-UCNPs*). UCNPs were synthesized according to the thermal decomposition method outlined by Mahaligham *et al.* [43]. Lanthanide trifluoroacetates were prepared from the corresponding oxides: 219.3 mg (0.93125 mmol) of Y_2O_3, 123.2 mg (0.3125 mmol) of Yb_2O_3 and 2.4 mg (0.00625 mmol) of Tm_2O_3, corresponding to a nominal composition $LiYF_4$: 25% Yb^{3+},0.5% Tm^{3+}. They were mixed in a 100 mL three necked round bottom flask along with 5 mL of distilled water and 5 mL of TFA. The slurry was refluxed under vigorous stirring at 80 °C until a clear solution was obtained. Then, the temperature was decreased to 60 °C and the residual TFA and water were allowed to slowly evaporate overnight. 2.5 mmol of LiTFA were added to the dried lanthanide trifluoroacetates together with 20 mL of OA and 20 mL of ODE. The mixture was degassed at 110 °C for 30 min and backfilled with Ar. The temperature was then raised to 330 °C and the reaction was allowed to proceed for 1 h. After this time, the heating was stopped and the flask was allowed to naturally cool down to 60 °C. The reaction product was split in two centrifuge tubes and the UCNPs were precipitated by the addition of ethanol. They were centrifuged (20 min at 6000*g*) and the supernatant was discarded. Eventually, the UCNPs were dispersed in hexane and washed three times with ethanol before being redispersed in toluene for further characterization.

Small $LiYF_4$:Yb^{3+},Tm^{3+} UCNPs (*s-UCNPs*). The procedure followed for the synthesis of smaller $LiYF_4$: 25% Yb^{3+},0.5% Tm^{3+} crystals was identical to the one described above, with the only exception of substituting 5 mL of OA with an equal volume of OLAm. The purification process of the UCNPs was the same as for *L-UCNPs.* The sample was eventually dispersed in toluene for further characterization.

Core/shell $LiYF_4$:Yb^{3+}/$LiYF_4$:Yb^{3+},Tm^{3+} UCNPs (*CS-UCNPs*). The trifluoroacetates for the synthesis of inactive-core/active-shell UCNPs were prepared respectively starting from: (i) *core:* 220.8 mg (0.9375 mmol) of Y_2O_3 and 123.2 mg (0.3125 mmol) of Yb_2O_3; (ii) *shell:* 219.3 mg (0.93125 mmol) of Y_2O_3, 123.2 mg (0.3125 mmol) of Yb_2O_3 and 2.4 mg (0.00625 mmol) of Tm_2O_3. These quantities correspond to a nominal composition $LiYF_4$: 25% Yb^{3+}/$LiYF_4$: 25% Yb^{3+},0.5% Tm^{3+}. Core UCNPs (*C-UCNPs*) were synthesized according to the procedure described for the synthesis of *L-UCNPs*. After 30 min of core growth, 2.5 mmol of lithium trifluoroacetate, 7.5 mL of OA, and 7.5 mL of ODE were added to the dried shell

precursors and the mixture was heated stepwise to 125 °C in 30 min under vacuum. After 1 h of core growth, 5 mL of the reaction mixture were taken and the shell solution was injected at a flow rate of 1.5 mL· min^{-1}. Once the injection was completed, the reaction was allowed to proceed for 1 h more. The purification steps were the same as reported for the other UCNP samples. *CS-UCNPs* UCNPs were eventually dispersed in toluene for further characterization.

CIS QDs. Copper-deficient CIS QDs were synthesized according to a simple thermal decomposition method. 9.5 mg of CuI (0.05 mmol), 58.4 mg of In(OAc)3 (0.2 mmol), 10 mL of ODE, 3.9 mL (16 mmol) of DDT and 0.708 mL (2 mmol) of OA were introduced in a 50 mL three-necked round bottom flask. The solution was stirred at 100 °C under vacuum for 45 min and backfilled with Ar. Then, the temperature was raised to 120 °C and maintained at this stage for 5 min. The temperature was further raised to 150 °C and maintained for 5 min more. Eventually, the temperature was set to 230 °C. Upon heating, the solution became completely clear and slightly yellow. Subsequently, the color changed from deep yellow to orange, then red and eventually dark red indicating the nucleation and growth of the QDs. After 45 min the flask was quenched in cold water. The QDs were transferred to a centrifuge tube and precipitated by the addition of acetone. They were centrifuged (20 min at 6000*g*) and the supernatant was discarded. The QDs were dispersed in toluene and washed twice with acetone, before being re-dispersed in toluene (approx. 0.15 mM) for further characterization.

Characterization techniques

Structure and morphology. The crystalline structure of the samples was probed by means of X-ray powder diffraction (XRPD) with a Bruker D8 Advance Diffractometer (Bruker, USA) using a Cu Kα radiation. The samples were prepared depositing few drops of the toluene sol of purified QDs or UCNPs on a glass slide and letting the solvent slowly evaporate in air. The morphology of the two structures was analyzed by means of transmission electron microscopy (TEM) and high-resolution TEM (HRTEM) using a JEOL JEM 3010 microscope (1.7 Å point to point resolution at Scherzer defocus) (JEOL, Japan). Before the imaging, each sample was further diluted in hexane to an approximate concentration of 0.1 mg/mL and sonicated for 2 min. One drop of the solution was deposited on a carbon-coated nickel grid and the solvent was allowed to slowly evaporate in air.

Optical properties. Absorption spectra were acquired on a Varian Cary 5000 spectrophotometer (Agilent, USA), diluting the QD sol in toluene to an optical density below 1 throughout the whole measurement range. PL and UCL spectra were collected at room temperature using a lens at an angle of 90° from the excitation beam and recorded with an Avaspec-ULS2048L spectrometer (Avantes, The Netherlands). QD and UCNPs emission were obtained under LED excitation at 450 nm (Thorlabs, USA) and laser diode excitation at 980 nm (BTW, China), respectively. In order to remove any stray light from the excitation sources, a short pass 785 nm filter and long pass 500 nm filter (Semrock, Inc., USA) were used in the two cases. The optical density of QD sol was kept below 0.1 at the excitation wavelength. The UCL spectra were recorded using sols of UCNPs at a concentration of 0.1 mg/mL. The relative PLQY of QDs was calculated using an aqueous solution of $Ru(bpy)_3Cl_2$ as a standard (emission peak: 613 nm, PLQY = 0.040 ± 0.002 [44]). For the optical measurements of dried samples, a home-made confocal fluorescence microscope was employed. A single-mode fiber coupled laser diode (980 nm) was used as the excitation source and focused on the sample with a microscope objective lens. Power densities on target varied between $1.4 \cdot 10^4$ W/cm^2 and $7.7 \cdot 10^4$ W/cm^2. The sample emission was collected through the same microscope objective. Emission and excitation light were discriminated by means of a dichroic mirror and a short-pass filter (FESH0950, Thorlabs, USA). The luminescence of the sample was collimated into the entrance of a high-resolution spectrometer (Horiba i320, Japan) and the signal was detected by a CCD detector (Synapse, Horiba, Japan). For LT measurements, samples were prepared casting a drop of sol of each UCNP batch on a glass slide and letting it dry in air. Concurrently, different amounts of CIS QDs were mixed with the UCNPs in toluene. A drop of the obtained sols was deposited on a glass slide. Each sample was excited by an optical parametric oscillator source (Spectra Physics, USA) at 960 nm (corresponding to the maximum absorption of Yb^{3+} ions in $LiYF_4$, see Figure S1). The UCL signal at 450 nm was filtered spectrally (FESH0750, Thorlabs, USA) and collimated into the entrance of a high-resolution spectrometer. The emission was amplified by a photomultiplier tube (R2949, Hamamatsu, Japan) and the UCL decay curves were recorded by means of a digital oscilloscope (LT372, LeCroy, USA).

Mathematical modelling of UCNP-QD FRET

The distinctive feature of FRET mechanism is its non-radiative nature, meaning that no emission of photons from the donor is involved but rather the energy is transferred according to a dipole-dipole type interaction between the two species [45]. One major requirement is that donor and acceptor should be in close proximity. The general expression to determine the Förster radius (R_0, *i.e.* the donor-acceptor separation R at which the FRET efficiency is 50%) is the following:

$$R_0^6 = \frac{9ln10\ PLQY\ \kappa^2 J}{128\pi^5 n^4 N_A} \qquad (1)$$

Where N_A is the Avogadro constant ($6.2 \cdot 10^{23}$ mol^{-1}), κ^2 is the dipole orientation factor, *PLQY* is the photoluminescence quantum yield of the donor, n is the refractive index of the medium and J is the spectral overlap integral:

$$J = \frac{\int f_D(\lambda)\epsilon_A(\lambda)\lambda^4 d\lambda}{\int f_D(\lambda) d\lambda} \qquad (2)$$

Where f_D is the spectral profile of the donor emission and ϵ_A is the molar extinction coefficient of the acceptor. Both acceptor and donor species in this study have been carefully designed in order to maximize the value of this last parameter, specifically choosing UCNPs whose emission largely overlaps with QD absorption. While J was obtained experimentally, two critical parameters in Equation 1 are the *PLQY* value and the dipole orientation factor κ^2. The effect of both parameters was therefore simulated (see next sections).

The efficiency of FRET scales with R^{-6} according to the following expression:

$$\eta = \frac{R_0^6}{R_0^6 + R^6} = 1 - \frac{\tau'_D}{\tau_D} \qquad (3)$$

As can be noticed, FRET efficiency can be experimentally determined from donor's LT values in the presence or absence of an energy acceptor (respectively τ'_D and τ_D). Using this approach, the average donor-acceptor distance was indirectly determined. Although we have until now referred to UCNPs when speaking about donors, it is important to mention here that the actual donor species are the optically active Tm^{3+} ions (activators). For this reason, when taking into account the donor-acceptor distance *R*, we will not refer to the UCNP-QD interparticle distance. More correctly, we will consider the distance between the QD surface and Tm^{3+} ions that are doped in the crystalline lattice of $LiYF_4$ and represent only a small fraction of the overall cations composing the crystal.

Results and discussion

Material characterization

CIS QDs were synthesized intentionally introducing a sub-stoichiometric amount of Cu^+ in the reaction environment. Although it is not clear yet how the presence of copper vacancies plays a role in the emission mechanism, Cu^+-deficient QDs display a higher PLQY with respect to the stoichiometric counterparts [46]. Synthesized QDs have a PLQY of 11% as obtained from the optical characterization (Figure S2A), which is in line with state of the art CIS QDs [47]. Their crystalline structure is the typical tetragonal chalcopyrite, as confirmed by the XRPD pattern (PDF #00-047-1372, Figure S2B). The morphology of the sample cannot be clearly distinguished from TEM observations, due to the poor contrast that this material gives under the electronic beam (Figure S2C). However, crystalline fringes are clearly observed from the micrographs, confirming the good crystallinity of the sample. From these images the diameter of the QDs is estimated to fall between 3 and 4 nm.

L-UCNPs, *s-UCNPs* and *CS-UCNPs* have a tetragonal crystalline lattice (PDF #01-078-2179), as confirmed from their XRPD patterns (Figures S3A, D, G). They have a bi-pyramidal habitus, which is characteristic of $LiYF_4$ (Figure 1A, C, E) [43,48] and are well crystallized, as can be inferred from the presence of extended crystalline fringes in HRTEM micrographs and strong diffraction spots in their electron diffraction patterns (Figures S3B, C, E, F, H, I and insets). The core/shell structure of *CS-UCNPs* is confirmed by the observation that this sample is composed of a single population of particles larger than parent core *C-UCNPs* (Figure 1E and inset, respectively). In order to geometrically describe the UCNPs, they were modelled as perfect square-based bi-pyramids and their characteristic lengths (*a* and *l*) were obtained from TEM micrographs (Figure S4). Statistical analysis shows that the growth of the shell takes place preferentially along the *a* axis rather than longitudinally along *l*. For the ease of modelling, also the shape of sample *CS-UCNPs* has been considered as bi-pyramid with sharp vertexes.

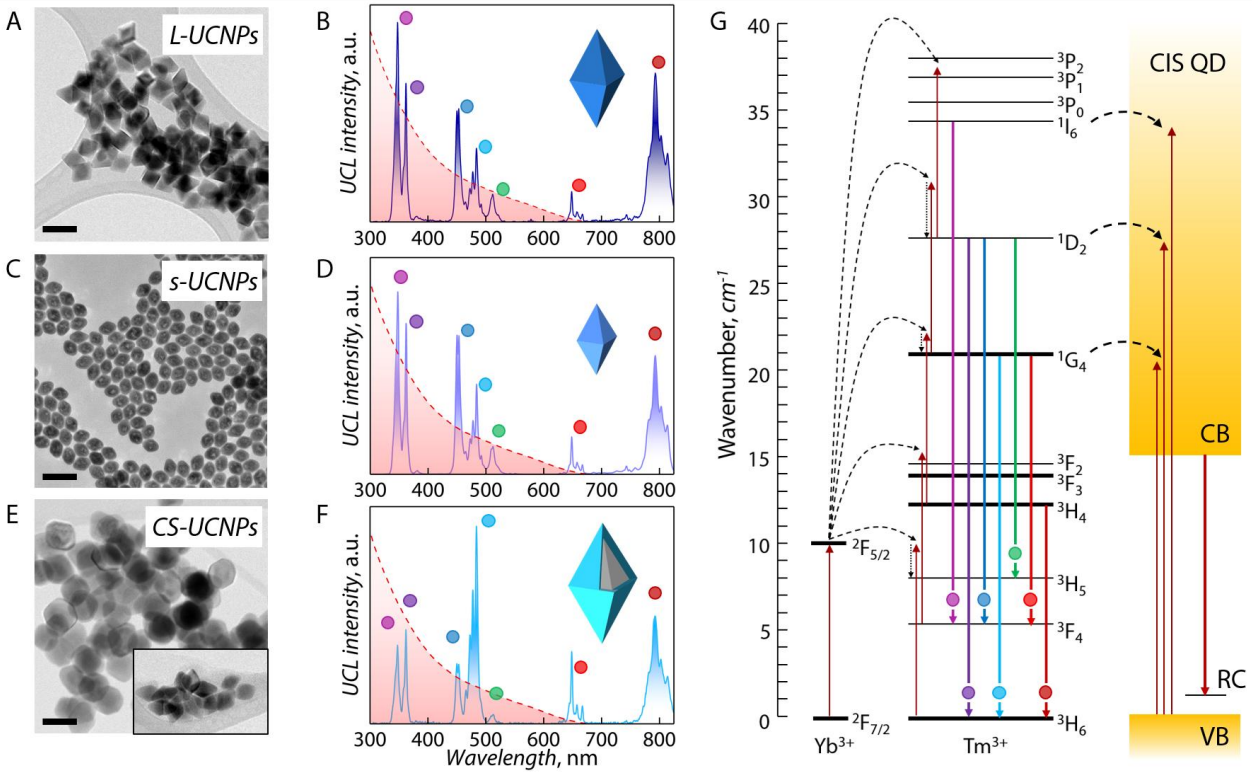

Figure 1. TEM micrographs show the three different UCNP architectures for *L-UCNPs* (A – core only), *s-UCNPs* (C – small core only) and *CS-UCNPs* (E – core/shell). Scale bars correspond to 100 nm. The different architecture is mirrored by the different UCL spectra of the three UCNP batches (B, D, and F, respectively; sketch of each UCNP architecture is illustrated as an inset) since smaller and core/shell UCNPs show less intense higher photon-order transitions, centered at shorter wavelengths. The absorption of CIS QDs (shaded red area in each UCL spectrum) largely overlaps with the UCL of the donors, setting the ground for an efficient FRET process. UCL spectra were recorded exciting at 980 nm, power density = 327 $W \cdot cm^{-2}$. The electronic level diagram of the Yb^{3+}-Tm^{3+} system is proposed (G), where the radiative transitions responsible for each emission band are depicted as solid colored arrows and correspondingly marked with a circle. QD's valence and conduction bands (VB and CB, respectively) are shown along with the energy transfer processes (dashed arrows) that are expected to take

place from the UCNP to the QD (RC is a recombination center). Legend: solid arrow - electron transition, dashed arrow - energy transfer, dotted arrow - non-radiative relaxation.

The dopant ion and the doping amount of UCNPs have been carefully chosen in order to maximize the overlap of their emission with the QDs' absorption, so to promote FRET. For this reason, $LiYF_4$ and Yb^{3+}/Tm^{3+} were selected respectively as the host material and the sensitizer/activator couple. All three batches of UCNPs display the characteristic emission lines of Tm^{3+} in $LiYF_4$, but the relative intensities of the bands vary considerably. In particular, the higher n^{th} photon order emissions (5^{th}: $^1I_6 \rightarrow {}^3F_4$ - 4^{th}: $^1D_2 \rightarrow {}^3H_6$, $^1D_2 \rightarrow {}^3F_4$) are markedly less intense in *CS-UCNPs* if compared with the 2^{nd} ($^3H_4 \rightarrow {}^3H_6$) and 3^{rd} photon order transitions ($^1G_4 \rightarrow {}^3H_6$, $^1G_4 \rightarrow {}^3F_4$). This behavior stems from the prevalently superficial distribution of Tm^{3+} ions throughout the particle volume. In *L-UCNPs* and *s-UCNPs* these optically active centers are homogeneously distributed over the entire crystal lattice, while in *CS-UCNPs* a larger percentage occupies sites close to the surface. This makes electron trapping in surface defect states more likely and fosters the interaction with solvent molecules, whose phonons promote non-radiative electron de-excitation from higher energy levels [49, 50]. Nevertheless, the larger fraction of superficial Tm^{3+} ions granted by the core/shell architecture represents a major benefit in the frame of FRET: there is a higher chance that an active center is close enough to an acceptor in contact with the UCNP's surface so that the non-radiative ET can take place. The same advantage is expected for small core-only UCNPs, since the higher surface-to-volume ratio of *s-UCNPs* with respect to *L-UCNPs* directly translates to an overall higher percentage of activators occupying a site in the proximity of the UCNP surface.

Study of transfer in sol

Initially, we investigated the possibility of observing the ET process in a homogeneous sol of UCNPs and QDs. The NPs composing the sol are subjected to the random phenomenon of Brownian motion [51]. The purpose of this study was to understand if and to what extent the ET mechanism takes place when the contact between the moieties is not favored (*e.g. via* surface modification) but is rather governed by stochastic events. Built on the observations made by Hong *et al.* [42] for the $NaYF_4:Yb^{3+},Er^{3+}/NaYF_4$-$CuInS_2/ZnS$ system, this investigation aimed to elucidate the mechanism of the observed ET. To do so, a 0.1 nM sol of *L-UCNPs* was prepared in toluene and the UCL signal was recorded exciting at 980 nm (power density = 327 $W \cdot cm^{-1}$), increasingly adding CIS QD sol in toluene or pure solvent (Figure 2A and S5, respectively). While the titration with the pure solvent did not lead to variations of the integrated UCL signal intensity, increasing the QD amount in the sol led to a steep decrease of the UCL intensity of the high order transitions (insets of Figure 2A and S5, respectively). This behavior could be explained in light of the spectral overlap between the UCNP emission and the QD absorption (Figure 1B). Even more interestingly, the integrated intensity of Tm^{3+}: $^1G_4 \rightarrow {}^3F_4$ line experienced an increase of approximately 15%, which followed from the appearance of the QD emission in the same wavelength range (Figure S2A). It is worth mentioning here that a similar behavior was observed for *CS-UCNPs* sample (Figure S6). Although the UCL quenching below 600 nm was comparable to the one observed in the case of *L-UCNPs*, the above-mentioned integrated intensity increase was barely appreciable (less than 4%) likely due to lower PLQY featured by *CS-UCNPs*. To confirm the postulated origin of the observed UCL intensity increase, a signal deconvolution was conducted [52] (refer to ESI for the thorough mathematical discussion). Specifically, the emission spectrum of each mixed sol (an example is shown in Figure 2B) was fitted, thus retrieving the QD emission in each case (Figure 2C and inset). The QD PL intensity integrated in the wavelength range of Tm^{3+}: $^1G_4 \rightarrow {}^3F_4$ transition was used to correct the UCL signal (inset of Figure 2A). Upon subtracting the QD contribution, the intensity of mentioned transition remains unchanged irrespective of the volume of acceptor sol added. The ET mechanism was interpreted combining the quantitative information about the QD emission and the estimation of the NP nearest neighbor distribution, as obtained from the sols' concentrations (Figure S7; the detailed mathematical discussion is reported in ESI). For each point, the integrated QD PL intensity was plotted against the first moment of the distribution (Figure 3). It was already mentioned that the typical FRET efficiency, and thus the acceptor's emission intensity, follows a R^{-6} dependence.

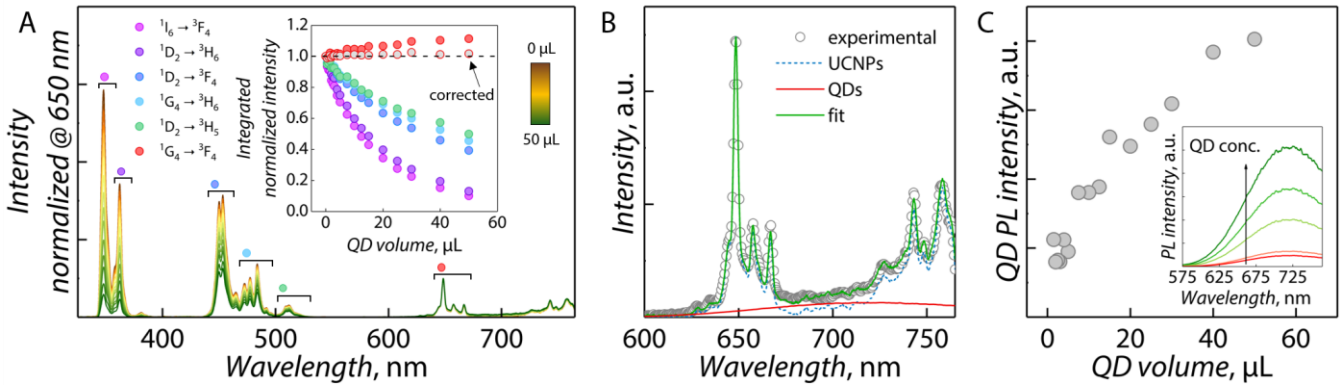

Figure 2. Upon titrating *L-UCNPs* sol with the CIS QD sol (A) the UCL signal decreases proportionally to the acceptor's concentration, as can be appreciated from the trend of the integrated normalized UCL intensity versus the QD sol volume added (inset in A). Nonetheless, Tm^{3+}: $^1G_4 \rightarrow {}^3F_4$ transition intensity increases, due to the appearance of the QD emission in that region. Deconvolution of the luminescence signal of the sols containing both UCNPs and QDs (B – highest QD sol volume tested) allowed to obtain the QDs' contribution to the spectrum of each mixed sol (C and inset). This information was used to correct the UCL Tm^{3+}: $^1G_4 \rightarrow {}^3F_4$ transition intensity from the mixed

sols (circles indicated by the arrow in inset of A). As could be anticipated from the minimal overlap of the Tm^{3+}: $^1G_4 \rightarrow {}^3F_4$ line with QDs' absorption, the UCL intensity in this region remained constant upon addition of increasing acceptor's amount. UCL spectra were recorded under excitation at 980 nm, power density = 327 $W \cdot cm^{-2}$.

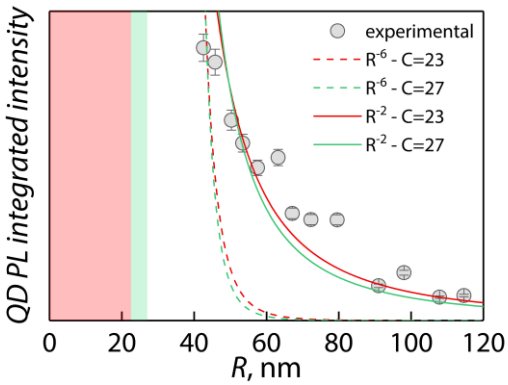

Figure 3. QD emission intensity was plotted versus the mean interparticle distance (R) that is ultimately the average donor-acceptor distance. The experimental points were fit using R^{-6} (dashed lines) and R^{-2} (solid lines) dependencies, respectively, typical for non-radiative and radiative energy transfer process. The better match obtained with the latter model confirms the radiative nature of the energy transfer phenomenon from UCNP to QD in sol. Shaded areas in the graphs represent the zones that are physically inaccessible for the acceptors when C = 23 (red) and C = 27 (green).

Instead, the efficiency of a radiative ET phenomenon decreases with the square of the distance and depends on the decay of the electromagnetic radiation in a medium. The mathematical model used to simulate these behaviors relies on the equation having the form:

$$I = \frac{B}{(R - C)^n} \qquad (5)$$

where R is the interparticle distance, n is an exponent that can either take value 2 (radiative ET) or 6 (FRET) and C is a geometrical factor that accounts for the steric hindrance, thus the impossibility of the NPs to spatially overlap (the choice of this value is discussed in ESI - Figure S8). B is a scaling parameter that was left free to vary during the fitting procedure. Equation 5 was used to fit the experimental data, observing that the radiative ET model better described the behavior of the system under study. This result is a strong indication of the nature of the ET process, although it does not completely exclude the possibility that a small fraction of the transferred energy could indeed be passed to the acceptors non-radiatively. This may occur in particular at higher concentrations tested, where the NPs are statistically closer Final evidence for the occurrence of FRET would come from the measurements of the donor's LT. However, such experiments failed to show any LT decrease, thus substantially ruling out the presence of FRET (Figure S9). It is to be mentioned that at high QD concentration (when FRET is expected to possibly become a competing transfer mechanism), the UCL signal was heavily quenched (up to 50-60%, see Figure 2B). This led to a poor signal-to-noise ratio, making the expected small - if any - FRET-induced LT changes not meaningful.

Study of transfer in dry powders

In order to establish the effect of different UCNP architectures on the mechanism of ET to QDs, the behavior of different combinations of the two species as dry powders was studied. To increase the likeliness of FRET events, the closest proximity between donors and acceptors was fostered by increasing the surface-to-volume ratio and preferentially segregating the active centers in the outer volume of the donors. Hence, three sets of samples were obtained, one for each type of UCNPs mixed with different CIS QD amounts. In all three cases, the lifetime of Tm^{3+}: $^1D_2 \rightarrow {}^3F_4$ transition experienced an appreciable shortening that allowed us to postulate a FRET-like mechanism taking place in this configuration (Figure 4A, B, C). At first inspection of the decay curves, *CS-UCNPs* and *s-UCNPs* both feature a slower decay rate than *L-UCNPs*. This difference between samples likely stems from difference in the samples' geometry, but is not relevant for the interpretation of the FRET mechanism (a thorough discussion on the subject is presented in ESI). The mean lifetime for each combination of UCNP-QD was evaluated from the integration of the normalized decay curves (Table 1). The curves were recorded for samples featuring a QDs-to-UCNPs ratio roughly up to 600. Experimental data suggest that it is possible to increase the efficiency of FRET by acting both on the size of the UCNPs and more directly on the distribution of the active ions throughout the donor's volume (Figure 4D). Specifically, in the presence of the highest amount of QDs, *s-UCNPs* and *CS-UCNPs* respectively experience a lifetime decrease of 32% in both cases, roughly double than the highest value (14%) observed for *L-UCNPs*. These values correspond to the FRET efficiency of each system according to Equation 3. In the case of CS-UCNPs, the LT decrease was steeper compared to the more gradual LT shortening in L- and s-UCNPs, and it could be observed starting from lower acceptor concentration.

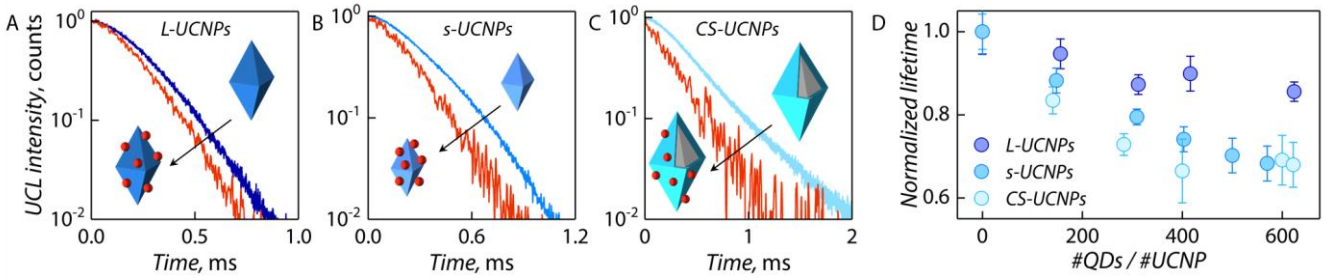

Figure 4. The mean Tm^{3+} $^1D_2 \rightarrow {}^3F_4$ transition LT in all UCNPs experienced a shortening in the presence of CIS QDs (A - *L-UCNPs*, B – *s-UCNPs*, C – *CS-UCNPs*). The UCNP LT monitored in the presence of increasing amount of QDs and normalized to that recorded in

absence of acceptors, showed a gradual shortening (D). The trend observed is not the same for the three batches, *L-UCNPs* being the UCNPs that showed the lesser degree of quenching considering comparable *#QD/#UCNP* values. This confirms that FRET efficiency can be increased with a proper UCNP design. Measurements were performed exciting at 960 nm.

Table1. The LT values in the absence (τ) and in the presence of the higher amount of QDs investigated (τ') were used to evaluate the FRET efficiency (η). The Förster radius (R_0) and the average donor-acceptor distance (R) were evaluated considering two κ^2 values: 0.67 is a usually accepted value used for randomly oriented dipoles, while 4 was chosen to compare the results with those obtained in the reference work from Bednarkiewicz *et al.* [39]. The percentage of Tm^{3+} ions present within the first 10 and 25 Å in the most superficial UCNP volume is the fraction of donors that can effectively give rise to FRET to nearby QDs. The errors associated to these values were derived *via* standard error propagation calculations using the uncertainties on the crystals' size as reported in Figure S4. This range of values is not reported for CS-UCNPs due to limitations on the calculation imposed by the particular morphology of the sample.

	τ, µs	τ', µs	η, %	$\kappa^2 = 0.67$		$\kappa^2 = 4$		*Tm^{3+} (10-25 Å)*, %
				R_0, Å	R, Å	R_0, Å	R, Å	
L-UCNPs	276 ± 15	237 ± 6	14 ± 2	13.7	18.5	18.5	25.0	(13 ± 4) - (29 ± 9)
s-UCNPs	325 ± 18	222 ± 14	32 ± 5	14.2	15.7	19.2	21.1	(18 ± 3) – (40 ± 7)
CS-UCNPs	477 ± 20	324 ± 26	32 ± 5	13.8	16.1	18.6	21.8	-

Indeed, the preferential segregation of Tm^{3+} ions at more superficial crystallographic sites in the core/shell architecture grants QDs an easier accessibility to this fraction of ions. Thus, the emission from these donors is masked by less unquenched signal stemming from non-superficial Tm3+ ions - which do not directly participate in the transfer mechanism. Therefore, in CS-UCNPs the optical information regarding LT values of Tm^{3+} ions involved in FRET to QDs is more readily accessible. In addition to the time-resolved measurements described above, spectral confirmation of FRET was also obtained. The UCL spectra of UCNPs alone and mixed with the highest amount of QDs investigated (Figures S10) showed that *s-UCNPs* and *CS-UCNPs* experience a dramatic UCL quenching in the short-wavelength side, which is accompanied by the appearance of the broad PL signal from QDs in the red spectral range.

A more complete picture was obtained considering how the abovementioned parameters are related to the geometry of the system and, specifically, the average distance between donor and acceptor (R). To do so, we explored how the Förster radius (R_0) varied depending on the value taken by each parameter of Equation 1. Here, we report the case of *L-UCNPs*, but the same procedure was applied to all types of UCNPs (results are reported in Figure S11). The intensity of the $^1D_2 \rightarrow {}^3F_4$ transition was normalized and the overlap integral (J) was evaluated considering the molar extinction coefficient of QDs (Figure 5A).

The effective refractive index, n, in the space separating the donor and the acceptor was considered to be 1.454, a value between the one of OA and DDT molecules covering the UCNPs' surface (1.459 for both compounds) and that of $LiYF_4$ (1.449). However, the effect exerted over the Förster radius (R_0) by the refractive index in this range is negligible (Figure S12). The variation of R_0 was eventually plotted as a function of *PLQY* (Figure 5B; κ^2 has little influence on R_0 in this system as shown in Figure S11D). A realistic range of *PLQY* value for the UCNPs was considered to be 0.001%-0.1% [53] while the dipole orientation parameter was allowed to take values from 0.67 to 4. The above reported results are in line with what has been shown by Bednarkiewicz *et al.* [39], although the R_0 values they obtained are slightly larger. This difference is tentatively ascribed to the better overlap between the selected UCL band and the QD's absorption realized here, thanks to the use of strongly blue-emitting Tm^{3+} instead of green-emitting Er^{3+}. As anticipated, the small R_0 values calculated for all UCNPs suggest that FRET takes place to the QDs from Tm^{3+} ions occupying the very first few nanometers of the crystal surface. Considering core-only UCNPs (*L-UCNPs*) the FRET efficiency is similar to that observed in the $NaYF_4$:Yb^{3+},Er^{3+}-CdSe QDs pair (14.8%). It has to be noted that Tm^{3+} is doped in the crystal lattice at four-fold dilution with respect to Er^{3+} [39,43]. However, remarkably we could more than double the FRET efficiency increasing the surface-to-volume ratio (*s-UCNPs*) and/or the active centers' distribution over the UCNP volume (*CS-UCNPs*).

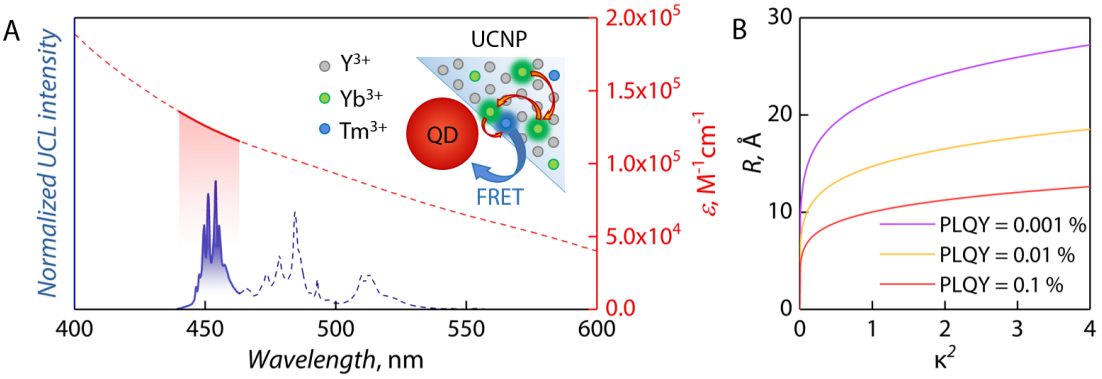

Figure 5. The normalized UCL of UCNPs and the molar extinction coefficient of QDs (A) were used to calculate the overlap integral (*J*); this value in turn was used to simulate the dependence of the Förster radius on the donor PLQY (B). The plots were obtained considering a refractive index n = 1.454, a value between 1.459 (OA and DDT) and 1.449 ($LiYF_4$). The inset in A depicts the suggested FRET mechanism from UCNP to QD prompted by NIR excitation of the donor (red/orange curved arrows represent energy migration events between Yb^{3+} ions and eventually to the emitting Tm^{3+} center).

It was argued that the dominant FRET mechanism is the transfer from one donor to one acceptor (QD) [39]. On the basis of this assumption, it was possible to estimate the fraction of Tm^{3+} ions in our system that can take part in the FRET mechanism. $LiYF_4$ has a tetragonal lattice where the ratio between the long and short edges of the unit cell (*c/a*) is close to 2 and each unit cell contains four formula units (*i.e.* 4 Li, 4 Y, 16 F). So one could consider the unit cell as composed of two cubic sub-cells of edge *a*, each containing two formula units. Taking a cell edge *a* = 5.2 Å (according to PDF #01-078-2179) it is possible to estimate the number of sub-cells in a single UCNP using the dimensions determined from TEM micrographs (values in Figure S4). Considering the case of *L-UCNPs* , the volume of a single UCNP is $7.39 \cdot 10^7$ $Å^3$, which gives $5.25 \cdot 10^5$ sub-cells per UCNP, corresponding to 5253 Tm^{3+} ions. Therefore, in the 10 to 25 Å of *L-UCNPs* outermost volume 13 to 29% of the donors can be found. This is the fraction of Tm^{3+} ions that is expected to predominantly contribute to FRET. This means that the majority of Tm^{3+} ions (from 87 to 71%) will not experience a LT shortening in the proximity to QDs and their emission will display the usual decay rate.

In smaller UCNPs (*s-UCNPs*) the fraction of active centers capable to effectively transfer the energy to nearby QDs is increased, compared to non-superficial Tm^{3+} ions. Following the same reasoning, a percentage of superficial Tm^{3+} ions ranging from 18 to 40% was estimated. These numbers are in good agreement with the efficiencies calculated from the UCL decay measurements. In the case of core/shell (*CS-UCNPs*) architecture, similar calculations could not be satisfactorily carried out due to the rather irregular morphology that prevented obtaining meaningful results. Reported results were obtained considering a *PLQY* of 0.01% for all the UCNPs. This is one of the most critical parameters in the considered system. Here, it is reasonable to assume that *L-UCNPs* feature somewhat higher emission efficiency with respect to *s-UCNPs*. This would translate to a smaller Förster radius in the latter UCNPs, thus a smaller fraction of superficial Tm^{3+} involved in the transfer mechanism (inset in Figure 5A shows the proposed FRET mechanism).

All considered, the results presented above unequivocally demonstrate that a rational design of the UCNP/donor architecture allows to obtain a remarkable improvement of FRET performance in pairs composed of UCNPs and QDs. Specifically, the UCNP size reduction and the localization of the activators preferentially in the outer UCNP volume have a comparable effect.

Conclusion

In this work, we studied the FRET phenomenon between $LiYF_4$:Yb^{3+}, Tm^{3+} UCNPs and $CuInS_2$ QDs. In particular, we investigated the effect of donor architecture on the process by either reducing the surface-to-volume ratio or segregating the dopant ions to the outer shell in a core/shell architecture. Initial studies in solution showed that the ET process was mostly radiative in nature. However, in the dry form, LT measurements demonstrated that FRET efficiency could be effectively increased acting both on the size of the UCNPs and more directly on the distribution of the active ions throughout the donor's volume. Both small and core/shell architectures featured a FRET efficiency (both 32%) more than doubled with respect to the reference UCNP sample (14%). Geometrical modelling of the donors showed a good match between the experimental results and the estimated fraction of superficial Tm^{3+} ions able to transfer their energy to nearby acceptors (QDs). These results highlight that FRET from UCNPs to QDs is indeed obtainable with a good efficiency when the energy donors are properly designed. These observations pave the way for the development of optical bio-assays that rely on the use of robust all-inorganic FRET pairs featuring NIR operational capabilities combined to a convenient long-lived emission.

ASSOCIATED CONTENT

Supporting Information. Description of squared residual minimization procedure; mathematical model for average interparticle distance in sol; interpretation of UCNPs' decay rate difference; absorption spectrum of UCNPs; characterization of UCNPs and CIS QDs; steady-state UCL of UCNPs mixed with CIS QDs; effect of PLQY, κ^2 and refractive index on FRET efficiency. This material is available free of charge via the Internet at http://pubs.acs.org.

AUTHOR INFORMATION

Corresponding Author

* Fiorenzo Vetrone, vetrone@emt.inrs.ca
* Daniel Jaque, daniel.jaque@uam.es

Present Addresses

† University of Ottawa, Department of Chemistry & Biomolecular Sciences, 10 Marie Curie St., Ottawa (ON) K1N 6N5, Canada

Author Contributions

The manuscript was written through contributions of all authors. All authors have given approval to the final version of the manuscript.

ACKNOWLEDGMENT

This work was supported by the Spanish Ministerio de Educación y Ciencia (MAT2016-75362-C3-1-R) and by COST Action CM1403. L.L.-P. thanks the Universidad Autónoma de Madrid for the ''Formación de Personal Investigador (FPI-UAM)'' program. P.H.-G. thanks the Spanish Ministerio de Economia y Competitividad for the Juan de la Cierva program (IJCI-2015-24551). A. Benayas thanks the Canadian Institutes of Health Research - Breast Cancer Society of Canada (CIHR-BCSC), for the support given to him through the *Eileen Iwanicki Postdoctoral Fellowship on Breast Cancer Imaging*. A. Benayas also thanks the European Commission, as his participation in this project at its later stage has received funding from the European Union´s Horizon 2020 research and innovation programme under the Marie Skłodowska Curie grant agreement No. 709270 "TEMPTATION". F. Vetrone is grateful to the Natural Sciences and Engineering Research Council (NSERC) of Canada for supporting his research.

REFERENCES

(1) Förster, T. Zwischenmolekulare Energiewanderung und Fluoreszenz *Annalen der Physik* **1948**, *437*, 55-75.

(2) Förster, T. Energiewanderung und Fluoreszenz *Die Naturwissenschaften* **1946**, *33*, 166-175.

(3) Bates, M.; Blosser, T. R.; Zhuang, X. Short-Range Spectroscopic Ruler Based on a Single-Molecule Optical Switch *Phys. Rev. Lett.* **2005**, *94*, 108101.

(4) Roy, R.; Hohng, S.; Ha, T. A practical guide to single-molecule FRET *Nat. Methods* **2008**, *5*, 507-516.

(5) González, J. E.; Tsien, R. Y. Improved indicators of cell membrane potential that use fluorescence resonance energy transfer *Chem. Biol.* **1997**, *4*, 269-277.

(6) Mere, L.; Bennett, T.; Coassin, P.; England, P.; Hamman, B.; Rink, T.; Zimmerman, S.; Negulescu, P. Miniaturized FRET assays and microfluidics: key components for ultra-high-throughput screening *Drug Discov. Today* **1999**, *4*, 363-369.

(7) Rodems, S. M.; Hamman, B. D.; Lin, C.; Zhao, J.; Shah, S.; Heidary, D.; Makings, L.; Stack, J. H.; Pollok, B. A. A FRET-based assay platform for ultra-high density drug screening of protein kinases and phosphatases *Assay Drug Dev. Technol.* **2002**, *1*, 9-19.

(8) Wallrabe, H.; Periasamy, A. Imaging protein molecules using FRET and FLIM microscopy *Curr. Opin. Biotechnol.* **2005**, *16*, 19-27.

(9) Sapsford, K. E.; Berti, L.; Medintz, I. L. Materials for fluorescence resonance energy transfer analysis: beyond traditional donor-acceptor combinations *Angew. Chem. Int. Ed. Engl.* **2006**, *45*, 4562-4589.

(10) Clegg, R. M. Fluorescence resonance energy transfer *Curr. Opin. Biotechnol.* **1995**, *6*, 103-110.

(11) Resch-Genger, U.; Grabolle, M.; Cavaliere-Jaricot, S.; Nitschke, R.; Nann, T. Quantum dots versus organic dyes as fluorescent labels *Nat. Methods* **2008**, *5*, 763-775.

(12) Shi, J.; Tian, F.; Lyu, J.; Yang, M. Nanoparticle based fluorescence resonance energy transfer (FRET) for biosensing applications *J. Mater. Chem. B* **2015**, *3*, 6989-7005.

(13) Piston, D. W.; Kremers, G. J. Fluorescent protein FRET: the good, the bad and the ugly *Trends Biochem. Sci.* **2007**, *32*, 407-414.

(14) Clapp, A. R.; Medintz, I. L.; Uyeda, H. T.; Fisher, B. R.; Goldman, E. R.; Bawendi, M. G.; Mattoussi, H. Quantum dot-based multiplexed fluorescence resonance energy transfer *J. Am. Chem. Soc.* **2005**, *127*, 18212-18221.

(15) Wang, L.; Tan, W. Multicolor FRET Silica Nanoparticles by Single Wavelength Excitation *Nano Lett.* **2006**, *6*, 84-88.

(16) Chen, N. T.; Cheng, S. H.; Liu, C. P.; Souris, J. S.; Chen, C. T.; Mou, C. Y.; Lo, L. W. Application of Time-Resolved Fluorescence for Direct and Continuous Probing of Release from Polymeric Delivery Vehicles *Int. J. Mol. Sci.* **2012**, *13*, 16598-16623.

(17) Hildebrandt, N.; Spillmann, C. M.; Algar, W. R.; Pons, T.; Stewart, M. H.; Oh, E.; Susumu, K.; Diaz, S. A.; Delehanty, J. B.; Medintz, I. L. Energy Transfer with Semiconductor Quantum Dot Bioconjugates: A Versatile Platform for Biosensing, Energy Harvesting, and Other Developing Applications *Chem. Rev.* **2017**, *117*, 536-711.

(18) Oh, E.; Hong, M. Y.; Lee, D.; Nam, S. H.; Yoon, H. C.; Kim, H. S. Inhibition assay of biomolecules based on fluorescence resonance energy transfer (FRET) between quantum dots and gold nanoparticles *J. Am. Chem. Soc.* **2005**, *127*, 3270-3271.

(19) Morales-Narvaez, E.; Merkoci, A. Graphene oxide as an optical biosensing platform *Adv. Mater.* **2012**, *24*, 3298-3308.

(20) Samia, A. C.; Chen, X.; Burda, C. Semiconductor quantum dots for photodynamic therapy *J. Am. Chem. Soc.* **2003**, *125*, 15736-15737.

(21) Skripka, A.; Valanciunaite, J.; Dauderis, G.; Poderys, V.; Kubiliute, R.; Rotomskis, R. Two-photon excited quantum dots as energy donors for photosensitizer chlorin e6. *J. Biomed. Opt.* **2013**, *18*, 078002.

(22) Wang, L.; Yan, R.; Huo, Z.; Wang, L.; Zeng, J.; Bao, J.; Wang, X.; Peng, Q.; Li, Y. Fluorescence Resonant Energy Transfer Biosensor Based on Upconversion-Luminescent Nanoparticles *Angew. Chem. Int. Ed. Engl.* **2005**, *44*, 6054-6057.

(23) Bhuckory, S.; Hemmer, E.; Wu, Y.-T.; Yahia-Ammar, A.; Vetrone, F.; Hildebrandt, N. Core or Shell? Er^{3+} FRET Donors in Upconversion Nanoparticles *Eur. J. Inorg. Chem.* **2017**, *2017*, 5186-5195.

(24) Muhr, V.; Wurth, C.; Kraft, M.; Buchner, M.; Baeumner, A. J.; Resch-Genger, U.; Hirsch, T. Particle-Size-Dependent Förster Resonance Energy Transfer from Upconversion Nanoparticles to Organic Dyes *Anal. Chem.* **2017**, *89*, 4868-4874.

(25) Deng, R.; Wang, J.; Chen, R.; Huang, W.; Liu, X. Enabling Förster Resonance Energy Transfer from Large Nanocrystals through Energy Migration *J. Am. Chem. Soc.* **2016**, *138*, 15972-15979.

(26) Del Rosal, B.; Ortgies, D. H.; Fernandez, N.; Sanz-Rodriguez, F.; Jaque, D.; Rodriguez, E. M. Overcoming Autofluorescence: Long-Lifetime Infrared Nanoparticles for Time-Gated In Vivo Imaging *Adv. Mater.* **2016**, *28*, 10188-10193.

(27) Weissleder, R. A clearer vision for in vivo imaging *Nat. Biotechnol.* **2001**, *19*, 316-317.

(28) Smith, A. M.; Mancini, M. C.; Nie, S. Bioimaging: second window for in vivo imaging *Nat. Nanotechnol.* **2009**, *4*, 710-711.

(29) Wang, F.; Deng, R.; Wang, J.; Wang, Q.; Han, Y.; Zhu, H.; Chen, X.; Liu, X. Tuning upconversion through energy migration in core-shell nanoparticles *Nat. Mater.* **2011**, *10*, 968-973.

(30) Xie, X.; Gao, N.; Deng, R.; Sun, Q.; Xu, Q. H.; Liu, X. Mechanistic investigation of photon upconversion in Nd^{3+}-sensitized core-shell nanoparticles *J. Am. Chem. Soc.* **2013**, *135*, 12608-12611.

(31) Skripka, A.; Marin, R.; Benayas, A.; Canton, P.; Hemmer, E.; Vetrone, F. Covering the optical spectrum through collective rare-earth doping of $NaGdF_4$ nanoparticles: 806 and 980 nm excitation routes *Phys. Chem. Chem. Phys.* **2017**, *19*, 11825-11834.

(32) Li, Z.; Zhang, Y.; Jiang, S. Multicolor Core/Shell-Structured Upconversion Fluorescent Nanoparticles *Adv. Mater.* **2008**, *20*, 4765-4769.

(33) Riuttamäki, T.; Hyppänen, I.; Kankare, J.; Soukka, T. Decrease in Luminescence Lifetime Indicating Nonradiative Energy Transfer from Upconverting Phosphors to Fluorescent Acceptors in Aqueous Suspensions *J. Phys. Chem. C* **2011**, *115*, 17736-17742.

(34) Wang, Y.; Shen, P.; Li, C.; Wang, Y.; Liu, Z. Upconversion fluorescence resonance energy transfer based biosensor for ultrasensitive detection of matrix metalloproteinase-2 in blood *Anal. Chem.* **2012**, *84*, 1466-1473.

(35) Wang, M.; Hou, W.; Mi, C. C.; Wang, W. X.; Xu, Z. R.; Teng, H. H.; Mao, C. B.; Xu, S. K. Immunoassay of Goat Antihuman Immunoglobulin G Antibody Based on Luminescence Resonance Energy Transfer between Near-Infrared Responsive $NaYF_4$:Yb, Er Upconversion Fluorescent Nanoparticles and Gold Nanoparticles *Anal. Chem.* **2009**, *81*, 8783-8789.

(36) Jesu Raj, J. G.; Quintanilla, M.; Mahmoud, K. A.; Ng, A.; Vetrone, F.; Zourob, M. Sensitive Detection of ssDNA Using an LRET-Based Upconverting Nanohybrid Material *ACS Appl. Mater. Interfaces* **2015**, *7*, 18257-18265.

(37) Nguyen, T. L.; Spizzirri, P.; Wilson, G.; Mulvaney, P. Tunable light emission using quantum dot-coated upconverters *Chem. Commun.* **2009**, 174-176.

(38) Yan, C.; Dadvand, A.; Rosei, F.; Perepichka, D. F. Near-IR Photoresponse in New Up-Converting CdSe/$NaYF_4$:Yb,Er Nanoheterostructures *J. Am. Chem. Soc.* **2010**, *132*, 8868-8869.

(39) Bednarkiewicz, A.; Nyk, M.; Samoc, M.; Strek, W. Up-conversion FRET from Er^{3+}/Yb^{3+}:$NaYF_4$ Nanophosphor to CdSe Quantum Dots *J. Phys. Chem. C* **2010**, *114*, 17535-17541.

(40) Mattsson, L.; Wegner, K. D.; Hildebrandt, N.; Soukka, T. Up-converting nanoparticle to quantum dot FRET for homogeneous double-nano biosensors *RSC Adv.* **2015**, *5*, 13270-13277.

(41) Doughan, S.; Uddayasankar, U.; Krull, U. J. A paper-based resonance energy transfer nucleic acid hybridization assay using upconversion nanoparticles as donors and quantum dots as acceptors *Anal. Chim. Acta* **2015**, *878*, 1-8.

(42) Hong, A. R.; Kim, J.; Kim, S. Y.; Kim, S. I.; Lee, K.; Jang, H. S. Core/shell-structured upconversion nanophosphor and cadmium-free quantum-dot bilayer-based near-infrared photodetectors *Opt. Lett.* **2015**, *40*, 4959-4962.

(43) Mahalingam, V.; Vetrone, F.; Naccache, R.; Speghini, A.; Capobianco, J. A. Colloidal Tm^{3+}/Yb^{3+}-Doped $LiYF_4$ Nanocrystals: Multiple Luminescence Spanning the UV to NIR Regions via Low-Energy Excitation *Adv. Mater.* **2009**, *21*, 4025-4028.

(44) Suzuki, K.; Kobayashi, A.; Kaneko, S.; Takehira, K.; Yoshihara, T.; Ishida, H.; Shiina, Y.; Oishi, S.; Tobita, S. Reevaluation of absolute luminescence quantum yields of standard solutions using a spectrometer with an integrating sphere and a back-thinned CCD detector *Phys. Chem. Chem. Phys.* **2009**, *11*, 9850-9860.

(45) Algar, W. R.; Kim, H.; Medintz, I. L.; Hildebrandt, N. Quantum Dots as Simultaneous Acceptors and Donors in Time-Gated Förster Resonance Energy Transfer Relays: Characterization and Biosensing *Coordin. Chem. Rev.* **2014**, *263-264*, 65-85.

(46) Kim, Y.-K.; Ahn, S.-H.; Chung, K.; Cho, Y.-S.; Choi, C.-J. The photoluminescence of $CuInS_2$ nanocrystals: effect of non-stoichiometry and surface modification *J. Mater. Chem.* **2012**, *22*, 1516-1520.

(47) Chen, B.; Zhong, H.; Zhang, W.; Tan, Z.; Li, Y.; Cairan, Y.; Tianyou, , Z.; Yoshio, B.; Shengyi, Y.; Bongsuo, Z. Highly Emissive and Color-Tunable $CuInS_2$-Based Colloidal Semiconductor Nanocrystals: Off-Stoichiometry Effects and Improved Electroluminescence Performance *Adv. Funct. Mater.* **2012**, *10*, 2081-2088.

(48) Wang, J.; Wang, F.; Xu, J.; Wang, Y.; Liu, Y.; Chen, X.; Chen, H.; Liu, X. Lanthanide-doped $LiYF_4$ nanoparticles : Synthesis and multicolor upconversion tuning *C. R. Chim.* **2010**, *13*, 731-736.

(49) Shao, W.; Chen, G.; Damasco, J.; Wang, X.; Kachynski, A.; Ohulchanskyy, T. Y.; Yang, C.; Agren, H.; Prasad, P. N. Enhanced upconversion emission in colloidal ($NaYF_4$:Er^{3+})/$NaYF_4$ core/shell nanoparticles excited at 1523 nm *Opt. Lett.* **2014**, *39*, 1386-1389.

(50) Johnson, N. J.; He, S.; Diao, S.; Chan, E. M.; Dai, H.; Almutairi, A. Direct Evidence for Coupled Surface and Concentration Quenching Dynamics in Lanthanide-Doped Nanocrystals *J. Am. Chem. Soc.* **2017**, *139*, 3275-3282.

(51) Pearle, P.; Collett, B.; Bart, K.; Bilderback, D.; Newman, D.; Samuels, S. What Brown saw and you can too *Am. J. Phys.* **2010**, *78*, 1278-1289.

(52) Marin, R.; Sponchia, G.; Zucchetta, E.; Riello, P.; Enrichi, F.; De Portu, G.; Benedetti, A. Monitoring the t → m Martensitic Phase Transformation by Photoluminescence Emission in Eu^{3+}-Doped Zirconia Powders *J. Am. Ceram. Soc.* **2013**, *96*, 2628-2635.

(53) Boyer, J.-C.; van Veggel, F. C. J. M. Absolute quantum yield measurements of colloidal $NaYF_4$: Er^{3+}, Yb^{3+} upconverting nanoparticles *Nanoscale* **2010**, *2*, 1417-1419.

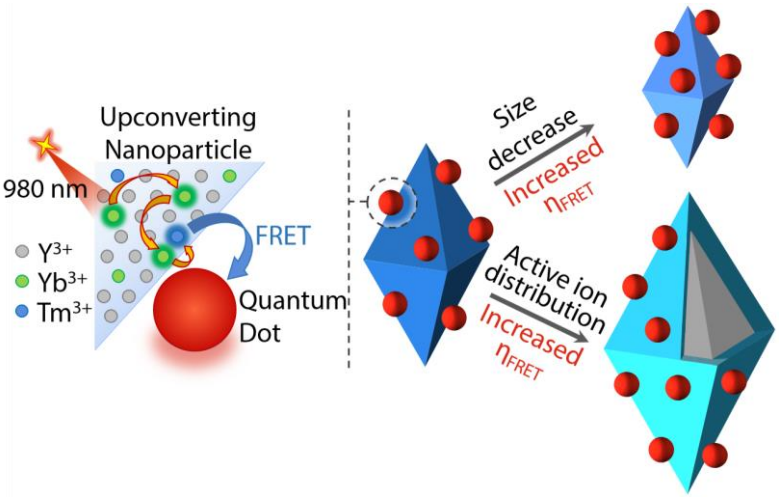

Decreasing the size of UCNPs and segregating the active ions in an outer shell allow to considerably increase the efficiency of FRET to QDs in a comparable way.